Northeast United States and Southeast Canada natural mercury emissions estimated with a surface emission model

Jesse O. Bash[*], David R. Miller, Thomas H. Meyer, Patricia A. Bresnahan

Department of Natural Resources Management and Engineering, University of Connecticut, 1376 Storrs Rd. Storrs, CT06269-4087, USA

Abstract

Most mercury emission inventories only include anthropogenic emissions and neglect the large contribution of the natural mercury cycle due to difficulty in spatially estimating natural emissions and uncertainties in the natural emissions process. The Mercury (Hg) Surface Interface Model (HgSIM) has been developed to estimate the natural emissions of mercury, for inclusion in a more complete mercury emissions inventory. The model used a 3422 cell, 36 km on each side, gridded domain and 1 h time steps. The emissions over land are modeled as a function of the land cover, evapotranspiration, and temperature. The emissions over water are modeled as a function of the concentration gradient, the mixing of the air and water, and the temperature.

The spatially distributed model is shown to account for the extreme spatial variability across the Northeast (NE) US and Southeast (SE) Canada. Estimates of natural mercury flux from uncontaminated surfaces are presented for a 2 week period in July. The total natural emissions for the domain, $4,434,912 \, \text{km}^2$, was $2101.5 \, \text{kg}$ over the 2 week simulation. The highest total natural emissions were $820 \, \text{ng} \, \text{m}^{-2}$ from the Atlantic Ocean in the SE part of the domain and the lowest total natural emissions were $74 \, \text{ng} \, \text{m}^{-2}$ in the urban areas with little vegetation. The flux estimates from vegetation canopies, averaged over the 14 days, ranged from $0.0 \, \text{ng} \, \text{m}^{-2} \, \text{h}^{-1}$ during the night time hours when transpiration ceased to $4.46 \, \text{ng} \, \text{m}^{-2} \, \text{h}^{-1}$ during the afternoon in a mixed deciduous–coniferous forest. The range of the air-water flux was between 0.5 and $2.73 \, \text{ng} \, \text{m}^{-2} \, \text{h}^{-1}$ over the model domain with the higher emission rates corresponding to windier and warmer areas. The soil emissions ranged from near 0 to $2.3 \, \text{ng} \, \text{m}^{-2} \, \text{h}^{-1}$ with the higher rates corresponding to warmer agricultural regions.

1. Introduction

Natural emissions and re-emissions of mercury have been estimated to be equivalent to anthropogenic mercury emissions when integrated spatially (Fitzgerald, 1995). Natural mercury emissions and re-emissions are greater than 99% Hg^0 due to its high vapor pressure at ambient conditions (Stein et al., 1996). The re-emissions of Hg^0 from terrestrial and aquatic ecosystems are an important, but not well documented, contribution to the atmospheric mercury cycle (Gardfeldt et al., 2001; Lamborg et al., 2002; Lindberg et al., 1998; Pirrone et al., 2001; Poissant and Casimir, 1998).

Recent measurements have documented natural emission pathways from soil, vegetation and water surfaces but show large variations in magnitude of emissions

*Corresponding author. Tel.: +1-860-486-1876; fax: +1-860-486-5408

E-mail address: jbash@canr.uconn.edu (J.O. Bash).

(Gardfeldt et al., 2001; Lindberg et al., 1998; Zhang et al., 2002). We hypothesize that much of this variation is due to spatial differences in the surface cover.

The emissions from soil surfaces appear to be driven by a chemical adsorption and desorption of mercury bound to soil particles (Zhang, 2001). Thus spatial variability of elemental mercury emission from soil can be expected to vary with the soil characteristics. Mercury concentrations in the transpiration stream of vegetation have been documented, and the measurement of mercury fluxes over vegetation canopies has indicated a stomatal control of the emissions (Bishop et al., 1998; Lindberg et al., 1998; Lindberg et al., 2002). Vegetative emissions appear to be an active process where mercury in the soil water solution is taken into the transpiration stream of the plant and subsequently emitted into the atmosphere (Bishop et al., 1998; Hanson et al., 1995; Lindberg et al., 1998). Therefore emissions in this pathway are dependent on vegetation cover. The air–water exchange of mercury is driven by turbulent diffusion (Gardfeldt et al., 2001; Rolfhus and Fitzgerald, 2001). In coastal marshes the vegetative pathway seems to dominate the transport (Lindberg et al., 2002) and the net flux seems to depend on the episodic availability of mercury in the sediments (Lee et al., 2000). Xu et al. (1999) modeled bi-directional exchanges from a portion of the Northeast (NE) United States and Southeast (SE) Canada and estimated average summer net emissions during hot, clear weather, of $22\,\mathrm{ng\,m^{-2}\,h^{-1}}$ from plant canopies and $2.6\,\mathrm{ng\,m^{-2}\,h^{-1}}$ from water surfaces.

The purpose of this research was to estimate regional natural emissions to the atmosphere from the NE United States and SE Canada by modeling the above processes which are described in various published studies. A spatially distributed numerical model was written to "scale up" the current experimental knowledge of Hg re-emissions pathways.

2. Methods

2.1. General approach

HgSIM models the natural emissions of elemental mercury from soils, vegetation, and water as independent emission sources and assumes they are the total emissions from a single area. Equations governing the emissions were derived from the literature and written in a computer program driven by meteorological data.

2.2. Emission pathway formulations

2.2.1. Emissions from transpiring vegetation

Elemental mercury emissions were calculated as the product of the transpiration rate and the concentration of the elemental mercury in the transpiration stream where the mercury in the transpiration stream is proportional to the soil water concentration (Bishop et al., 1998; Hanson et al., 1995).

$$F_S \propto EC_S, \tag{1}$$

Where F_S is the flux of mercury from the canopy in $\mathrm{ng\,m^{-2}\,h^{-1}}$, E is the transpiration rate in $\mathrm{kg\,m^{-2}\,h^{-1}}$, and C_S is the concentration of elemental mercury in the soil water in $\mathrm{ng\,kg^{-1}}$.

Canopy transpiration is modeled using the Penman-Monteith conductance model, with a stomatal conductance algorithm based on Jarvis (1976) and Stewart (1988).

$$E_t = \frac{s(R_n - G) + c_p g_H D/p}{\lambda \left(s + \frac{c_p g_H}{\lambda g_v}\right)}, \tag{2}$$

Where E_t is the transpiration in $\mathrm{kg\,m^{-2}\,s^{-1}}$, s is the slope of the saturation vapor pressure temperature curve, R_n is the net radiation, p is the atmospheric pressure, G is the soil heat flux, D is the saturation vapor pressure deficit, $D = e_s(T) - e_a$, $e_s(T)$ is the saturation vapor pressure as a function of temperature and e_a is the ambient air vapor pressure. c_p is the specific heat of water, λ is the latent heat of vaporization, g_H is the boundary layer conductance and g_v is the total vapor conductance. All of the weather parameters for Eq. (2) (R_n, p, T, e_a), and for the following equations, were estimated from the Mesoscale Meteorology Model (MM5) modeled results for the surface layer.

The boundary layer conductance is calculated following Campbell and Norman (1998) and Stull (1988),

$$g_H = \frac{k^2 \rho u(z)}{\left[\ln\left(\frac{z-d}{z_M}\right) + \Psi_M\right]\left[\ln\left(\frac{z-d}{z_H}\right) + \Psi_H\right]}, \tag{3}$$

where k is the von Karman constant, ρ is the density of the air, z is height from the surface, $u(z)$ is the wind speed at height z, d is the zero plane displacement, z_M is the momentum roughness length, z_H is the roughness length for heat, Ψ_M is the diabatic correction factor for momentum, and Ψ_H is the diabatic correction factor for heat. z, d, z_M, and z_H were estimated from the land use cover.

The total vapor conductance was modeled following Campbell and Norman (1998).

$$g_v = \frac{g_H + g_s}{g_H g_s}, \tag{4}$$

where g_s is the stomatal conductance.

The stomatal conductance is a nonlinear function of solar radiation, R_s, specific humidity deficit, δq, temperature, T, and soil moisture deficit, $\delta \theta$. Functions of these variables range from zero to unity and the conductance is modeled as the product of these functions, leaf area index (LAI), and the maximum stomatal conductance for the modeled vegetation type,

K_{max} (Jarvis, 1976; Stewart, 1988).

$$g_s = LAIK_{max}g(R_s)g(\delta q)g(T)g(\delta\theta). \qquad (5)$$

2.2.2. Emission from Surface Water

Emissions from surface waters are defined as turbulence-enhanced. This process is modeled using a two-film turbulent diffusion coefficient and the divergence from the air–water equilibrium concentrations.

$$\frac{1}{k_l} = \frac{1}{K_l} + \frac{1}{K_g H}, \qquad (6)$$

where K_g is the gas side transfer coefficient, K_l is the liquid side transfer coefficient, k_l is the overall transfer coefficient, and H is the dimensionless Henry's constant (Thomann and Mueller, 1987). The overall turbulent transfer coefficient is parameterized as a function of wind speed modeled after Wanninkhof (1992).

$$k_l = 0.31 U_{10}^2 (Sc_{Hg}/Sc_{CO_2})^{-1/2}, \qquad (7)$$

where U_{10} is the wind speed at 10/m and Sc_{Hg} and Sc_{co_2} are the Schmidt numbers for mercury and carbon dioxide, respectively. The net flux (F_w) is then the difference between the elemental mercury concentration of the surface water and the equilibrium concentration of mercury in water for the atmospheric concentration.

$$F_w = k_l(C_w - C_a/H), \qquad (8)$$

where Ca is the atmospheric concentration of Hg^0 and C_w is the aqueous Hg^0 concentration. Eq. (8) may also be represented as the difference of the emission rate of elemental mercury from the water surface, Eq. (9), and the dry deposition rate of mercury onto the water surface, Eq. (10).

$$F_e = k_l C_w, \qquad (9)$$

$$F_d = k_l C_g/H. \qquad (10)$$

The partitioning of elemental mercury between the water and atmospheric phases is given by Henry's constant.

$$H = \frac{p_{hg,eq}}{X_{Hg}}, \qquad (11)$$

where $p_{Hg,Eq}$ is the equilibrium partial pressure of mercury in the atmosphere and X_{Hg} is the mole fraction of Hg^0 in the water (Rolfhus and Fitzgerald, 2001; Thomann and Mueller, 1987). Henry's constant is parameterized as a unitless function of temperature following Sanemasa (1975).

$$H = \frac{M_w\left(10^{\frac{-1078}{T_s}+6.25}\right)}{R\rho_w T_s}, \qquad (12)$$

Where M_w is the molar weight of water ($kg\,mol^{-1}$), R is the gas constant ($atm\,dm^3\,K^{-1}\,mol^{-1}$), ρ_w is the density of water ($kg\,dm^{-3}$), and T_s is the temperature at the air–water interface (K).

2.2.3. Emissions from soil

The air–soil flux of mercury may be considered as the adsorption/desorption of Hg from/to soil particles and the subsequent diffusion through soil pores (Zhang, 2001). The reaction rate constant for the above process is often related to surface temperature by Arrhenius-type equations (Carpi and Lindberg, 1998; Poissant and Casimir, 1998; Zhang, 2001).

$$k_s = A\mathrm{Exp}\left[\frac{-E_a}{RT_s}\right], \qquad (13)$$

where E_a is the activation energy, T_s is the soil temperature, R is the universal gas constant, and A is a regression constant. The soil Hg concentration is assumed to remain relatively constant over the simulation period, thus the reaction can be modeled as a zero order reaction and the flux can be modeled as a function of temperature alone (Zhang, 2001). Due to the lack of available soil Hg concentrations, the soil emissions were modeled following Carpi and Lindberg (1998) for a background soil.

$$F_s = 10^{aT_s+b}, \qquad (14)$$

where F_s is the mercury emissions from the soil and the regression constant a and b are 0.064 and -2.03, respectively (Xu et al., 1999).

2.2.4. Data Flow in HgSIM

The HgSIM program is configured using environmental variables and text files. Data that is used by more than one subroutine is stored in shared memory to eliminate redundant calculations and input routines. The details of HgSIM operation are reported in Bash (2003).

2.3. Simulations

HgSIM was programmed in Fortran 90 on a Sun Ultra 60® workstation using the Forte Workshop® compiler suit. The USEPA Models-3 IO/API libraries were used to ensure compatibility with the Community Multiscale Air Quality (CMAQ) and the Sparse Matrix Operation Kernel Emissions (SMOKE) models. The output is in Network Common Data Format (NetCDF), a self describing, direct access binary format that is portable between operating systems. The meteorological boundary conditions are resolved using the University of North Carolina Computer Modeling and Analysis System's (CMAS) Meteorology Chemistry Interface Processor (MCIP).

All dynamic weather and land surface conditions are provided by Mesoscale Model 5 (MM5) (Grell et al., 1994).
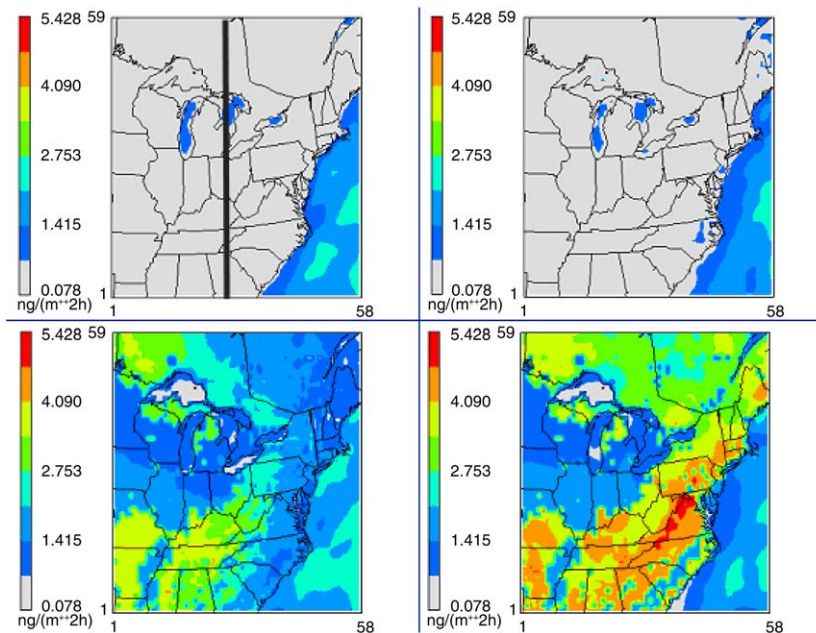
Fig. 1. 2-week hourly average mercury emissions for a July day clockwise from the top left corner at 5:00 GMT, 11:00 GMT, 17:00 GMT, 23:00 GMT (24:00 EST, 6:00 EST, 12:00 EST, 18:00 EST). The location of the transect shown in Fig. 2 is displayed in the 5:00 GMT panel.

The modeling domain covers the NE United States, SE Canada, and parts of the Northern Atlantic Ocean as shown in Fig. 1. The horizontal plane consisted of 58×59 rows by columns on a Lambert conformal conic map projection centered over $40°$ longitude north and $75°$ latitude west. The vertical depth of this layer is approximately 30 m and rises from the modeled surface. The model was run using hourly meteorological data from the Mesoscale Model 5 version 2 (MM5v2). The MM5 data was processed using the Meteorological Chemistry Interface Processor version 2 (MCIP2) to calculate the appropriate variables and convert the meteorological data into the Models-3 IO/API format. The spatial attributes of the model domain used a simple fractional coverage with 11 categories of surface data parameterizations, identical to that used by MCIP2. The simulation presented in this paper estimated emissions from 0:00 GMT July 6th 1997 to 23:00 GMT July 19th 1997.

The initial concentrations were taken from clean background values reported in current literature and were assumed to be constant over the short modeling period, (Table 1). Ambient concentration values only affected the air–water Hg^0 flux, and the average values for ambient and aqueous concentrations during the summertime over the North Atlantic were used (Xu et al., 1999). It was assumed that the majority of the modeling domain was rural, thus relatively clean

concentrations were used for terrestrial systems (Bishop et al., 1998; Xu et al., 1999).

2.4. Spatial Variability

To generalize the spatial patterns and quantify the spatial variability across the entire domain we calculated directional, semivariograms after Isaaks and Srivastava, (1989) for each hour in the diurnal cycle. A semivariogram is a measure of the spatial variability present in an autocorrelated data set (s). $s_i \in R$ denotes a particular element from the set of samples, S, where R denotes the set of real numbers. The samples are assumed to have been collected at distinct locations, e.g., $p_i = (x_i, y_i)$ for sample s_i. Defining h as a non-negative real number called a "lag distance," $P(h) = \left\{ (p_i, p_j) \| p_i - p_j \| = h \right\}$, where $P(h)$ is the set of sample pairs that are separated by a planimetric distance h. Then, the semivariogram of S is

$$\gamma(h) = \frac{1}{2N} \sum_{(p_i, p_j) \in P(h)} (s_i - s_j)^2, \qquad (15)$$

where N is the number of elements in $P(h)$.

More specifically, Eq. (15) is called an *omni-directional semivariogram* because h, being a scalar, stipulates that P contains all pairs of samples separated by a constant distance but without consideration of direction. If the

Table 1
Assumed values and constants

Hg^0 concentration in soil water (ng l^{-1})	100	Xu et al. (1999)
Hg^0 concentration in sea water (ng l^{-1})	0.04	Xu et al. (1999)
Soil water deficit (mm)	5	Xu et al. (1999)
Ambient Hg^0 concentration over the north Atlantic (ng m^{-3})	2.5	Poissant and Casimir, (1998)
Hg^0 concentration in the transpiration stream (ng l^{-1})	12.3	Bishop et al. (1998)
Hg concentration in the soil media (µg m^{-3})	0.22	Gillis and Miller (2000)
LAI's (m^2 m^{-2})	Full canopy healthy species averages	Beld2 configuration scripts

definition of P is generalized by defining the lag to be a vector $\mathbf{h}$, then $P(\mathbf{h}) = \left\{ (p_i, p_j) | p_i - p_j = \mathbf{h} \right\}$, and Eq. (15) becomes

$$\gamma(\mathbf{h}) = \frac{1}{2N} \sum_{(p_i, p_j) \in P(\mathbf{h})} (s_i - s_j)^2, \qquad (16)$$

where N is the number of elements in $P(\mathbf{h})$.

From Eq. (16) it is clear that $\gamma(0) = 0$ and that $\gamma(h) \geqslant 0$. Therefore, one expects that the semivariogram of an autocorrelated data set is relatively small for small lags and increases as the lag increases. This follows the notion that decorrelation occurs with separation: large values of $\gamma(h)$ indicate large variability and vice versa.

3. Results

3.1. Estimates of Fluxes

HgSIM was run for a 2-week simulation period from July 6th 1997 to July 19th 1997. The total emission calculated for the 2-week period for the entire domain was 2101.5 kg. The HgSIM model predicted a spatially averaged daily maximum emission rate of mercury from vegetation of 4.4 ng m^{-2} h^{-1}, a daily maximum average emission rate from soil of 2.3 ng m^{-2} h^{-1} and a daily maximum average positive flux of mercury from surface waters of 2.7 ng m^{-2} h^{-1}. The maximum fluxes for all three pathways occurred in the early to late afternoon and the minimum values, ~ 0 ng m^{-2} h^{-1} for all three modeled pathways, occurred in the early to mid-morning.

Fig. 1 maps the mercury flux spatial and time variability across the computational domain. The maximum and minimum terrestrial emissions corresponded with the maximum and minimum ambient temperatures, respectively. The highest overall rate of emissions came from the southern portion of the modeled domain. However, during the afternoon peak, the spatial variability of Hg^0 fluxes for terrestrial systems was at its maximum in the northern parts of the domain. Over the 2-week simulation the highest total natural emissions were 820 ng m^{-2} from the Atlantic
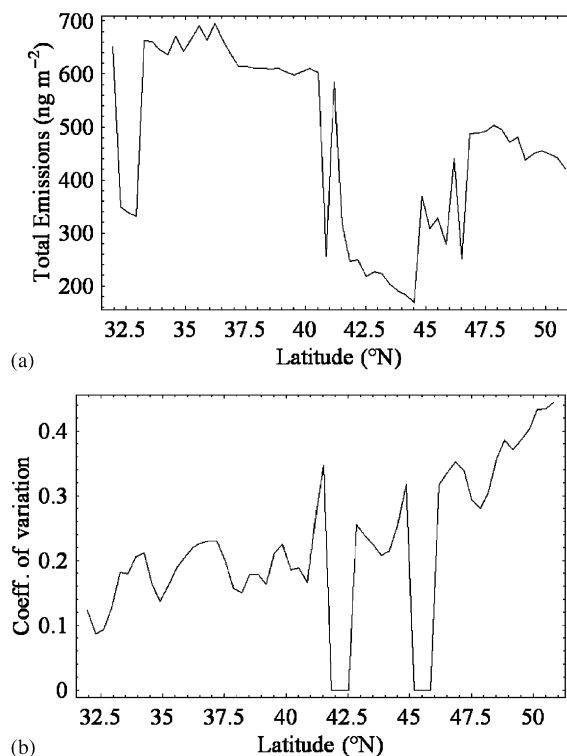
Fig. 2. (a) Total estimated Hg^0 emissions for the 2-week simulation along a south to north transect; (b) the coefficient of variation in Hg^0 emissions from vegetation for the north–south transect at 12:00 over the 2-week simulation period.

Ocean off the Southeast coastline and the lowest total natural emissions were 74 ng m^{-2} in the urban areas with little vegetation cover around Washington D.C.

3.2. Spatial patterns in modeled Hg^0 emissions

Spatial patterns of emissions along a north–south transect, from (31.96°N, 82.87°W) to (50.84°N, 80.19°W), across the model domain can be seen in Fig. 2. The high emission variability shown is due to variations in land cover type.

Emissions from mixed deciduous-coniferous forest sites in North Carolina and Quebec are shown in Fig. 3 to demonstrate the effects of latitude on vegetation and soil emissions of elemental mercury.

The estimated vegetation and soil emissions were higher for the North Carolina site for almost all of the time periods in the simulation, (Fig. 3a,b). The average

(a)

(b)

(c)
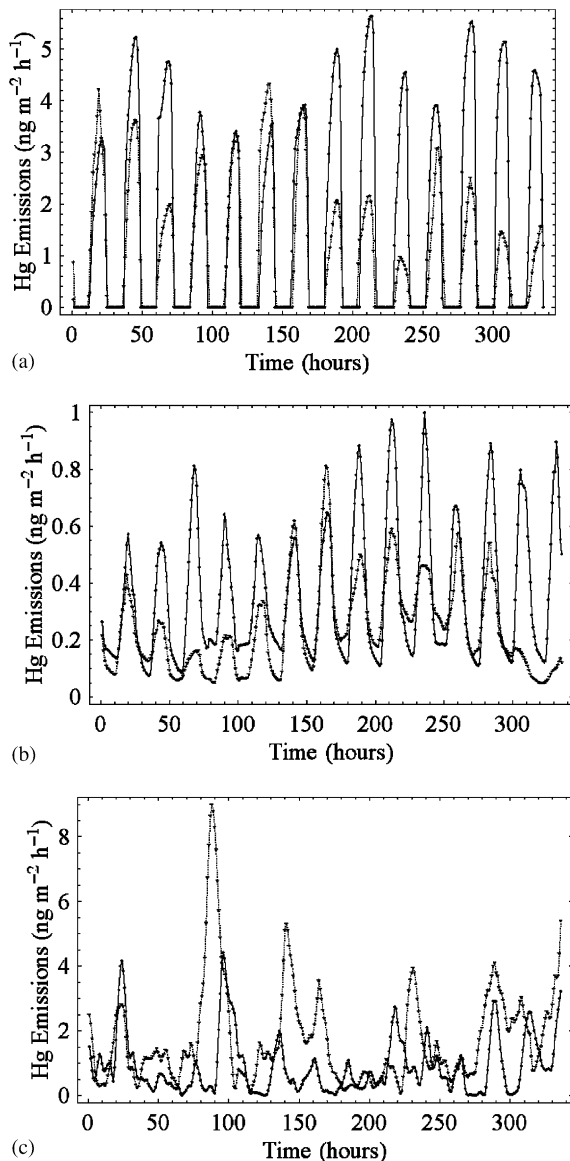
Fig. 3. (a) Estimated vegetation Hg^0 emissions from a mixed hardwood forest in North Carolina (solid line) and Quebec Canada (dotted line); (b) Estimated Hg^0 soil emissions from a mixed deciduous–coniferous forest floor from North Carolina (solid line) and Quebec Canada (dotted line); (c) Estimated Hg^0 air–water flux over water off the coast of Alabama (solid line) and Maine (dotted line)

estimated emissions over the 2 week period was $1.61\,ng\,m^{-2}\,h^{-1}$ for the North Carolina site and $0.96\,ng\,m^{-2}\,h^{-1}$ for the Quebec site. The estimated soil emissions for the North Carolina site were greater than that of the Quebec site with average modeled emissions rates for the 2-week simulation of $0.36\,ng\,m^{-2}\,h^{-1}$and $0.24\,ng\,m^{-2}\,h^{-1}$, respectively.

A spatial trend in the air–water flux was less evident than in the terrestrial fluxes in the model output, (Fig. 3c). This is due to the strong influence of wind speed and the warm gulf-stream current on the air–water flux emissions. The average modeled fluxes off of the coast of Maine were higher than the average modeled flux off of the coast of South Carolina with rates of $1.78\,ng\,m^{-2}\,h^{-1}$ and $0.92\,ng\,m^{-2}\,h^{-1}$, respectively.

3.3. Temporal patterns in modeled Hg^0 emissions

The estimated vegetation and soil emissions followed strong diurnal patterns for both an average day, (Fig. 1), and individual days (Figs. 3a,b). Mesoscale meteorological events effected both the vegetation and soil emissions over periods greater than a day. The temporal pattern of the air–water flux is much less defined due to its high dependence on wind speed and water temperature, (Fig. 3c).

4. Discussion

Modeled natural Hg^0 emissions are compared to published measured net emission data from the NE US and SE Canada regions and similar climates in Table 2. The emissions from vegetation canopies estimated here were generally lower than the published measurements of Lindberg et al. (1998), Lindberg et al., (2002) but similar to the published measurements of Hanson et al.,(1995). We expect that within-grid averaging of land cover in the model generally results in lower emission rates from the model when compared to point measurements.

4.1. Emission Pathways

The average vegetation emissions rates for forested regions were roughly twice that of the soil or water emission rates during times of peak transpiration (Fig. 1). Foliar emissions rates were larger than those of water or soil due to the assumption that mercury is actively being transported in vegetative transpiration processes. The vegetation and soil emissions exhibit a strong diurnal pattern with lower emissions at night (Fig. 3a,b), while the emissions from water do not exhibit as strong a diurnal trend (Fig. 3c). Therefore, the total emissions from the water over the two week period were estimated to be roughly equal to that of vegetation emission from heavily forested areas.

Table 2
HgSIM estimates of mercury emissions and some other published measurements

Emission source	Hgsim estimates	Published data	Source
VEGETATION			
Hardwood forest	4.46 ng m^{-1} h^{-1}		Average maximum 12:00 flux
Mixed agriculture	3.1 ng m^{-1} h^{-1}		Average maximum 12:00 flux
Mature hardwood, TN		8–66 ng m^{-1} h^{-1*}	Lindberg (1998)
Young pines, TN		1–35 ng m^{-1} h^{-1*}	Lindberg (1998)
Cattail canopy, FL		17 ± 43 ng m^{-1} h^{-1}	Lindberg et al. (2002)
Red maple (Acer rubrum L.)		5.5 ng m^{-1} h^{-1}	Hanson et al. (1995)
Norway spruce (Picea abies L.)		1.7 ng m^{-1} h^{-1}	Hanson et al. (1995)
Yellow-poplar (Liriodendron tulipifera L.)		2.7 ng m^{-1} h^{-1}	Hanson et al. (1995)
White oak (Quercus alba L.)		5.3 ng m^{-2} h^{-1}	Hanson et al. (1995)
SOIL			
Forest floor	1.5 ng m^{-1} h^{-1}		Average maximum 12:00 flux
Agricultural regions	2.3 ng m^{-1} h^{-1}		Average maximum 12:00 flux
Sweden		0.4-1.8 ng m^{-1} h^{-1}	Lindberg (1998)
Oak ridge, TN			
Shaded forest soil		2-7 ng m^{-1} h^{-1}	Carpi and Lindberg (1998)
Shaded forest soil, MI		1.4 ± 1.4 ng m^{-1} h^{-1}	Zhang (2001)
Southern quebec, agricultural		3 ± 2.2 ng m^{-1} h^{-1}	Poissant and Casimir (1998)
WATER			
Atlantic ocean	2.73 ng m^{-1} h^{-1}		Average maximum 12:00 flux
Great lakes	1.5 ng m^{-1} h^{-1}		Average maximum 12:00 flux
Mediterranean sea		0.7–11.25 ng m^{-1} h^{-1}	Pirrone et al. (2001)
Sweden		2.81 ± 0.69 ng m^{-1} h^{-1}	Gardfeldt et al. (2001)
Long island sound		0.27–5.3 ng m^{-1} h^{-1}	Rolfhus and Fitzgerald (2001)

Emissions from soils were estimated to range from ∼20% of the terrestrial emissions for southern forested areas to 25% for northern forested areas. In agricultural regions, the soil emissions were estimated to be as high as 75% of the total terrestrial emissions in the southern regions and 65% for the northern regions. Emission rates from soils were lower in forests than agricultural lands due to the insulating effect the forest canopies had on the forest soils.

4.2. Time variations

Figs. 3a,b demonstrate that temporal variations occur on both a diurnal cycle and a larger synoptic cycle as weather systems pass over the modeled regions.

Spatial and temporal variation is most evident in the interaction of precipitation events with the energy balance time series. Precipitation events passed over the North Carolina site on the 1st, 5th, and 11th day of simulation and over the Quebec site on the 2nd, 11th, and 13th day of simulation. The precipitation in Quebec came with considerably more cloud coverage. The reduction in the available energy due to the precipitation events resulted in a reduction of transpiration and mercury emissions. Some measurements have indicated higher Hg emissions immediately after a rain event (Gustin and Lindberg, 2000) and soil wetting (Gillis and Miller, 2000). This is not reflected in the model because mechanisms and variability for this process have yet to be defined.

4.3. Spatial variations

Finding global and regional total fluxes in various parts of the global mercury cycle is a major objective of most ongoing environmental mercury research. The importance of scaling-up has been previously pointed out by Lindberg et al. (2002) and the pioneering work of Lindberg and colleagues in measuring natural fluxes in various systems has given us most of the available data sets which demonstrate the transpiration pathway. Directly "scaling-up" limited experimental information to large regions involves essentially linear extrapolations and assumptions about the uniformity of the process across regions and vegetation types. Intuitively we suspect that global estimates from limited

point measurements are likely to result in large errors in a process as complicated as natural mercury emissions. For example, Fig. 2 shows large spatial variations in magnitude and variability due to land use and location in the modeled domain. Using a linear extrapolation technique from any point in the transit in Fig. 2a to produce an average, or total, for the entire transit is an obstinate problem because the space series is not homogeneous (Fig. 2b) nor normally distributed.

Here, we use HgSIM, to "scale-up" emissions to the entire NE US and SE Canada region. Assumptions about spatial distributions are only necessary on scales smaller that the model grid size, in this case 36 km. At larger scales the variations in surface characteristics are directly used in the flux calculations. In this study we used the spatially distributed flux across the computational domain to quantify the spatial variability, and time–space interaction of that variability.

Twenty-four semivariograms of natural mercury flux, one for each hour of the diurnal cycle, were calculated using the model output averaged over 14 days. Fig. 4 shows directional semivariograms of mercury flux for the calculation domain for the 4 h previously shown in Fig. 1. The figure graphs variance as a function of lag distance and direction. The directions plotted are in increments of $\pi/18$, e.g. 0, $\pi/18$, $\pi/9$, ... , $17\pi/18$, where 0 is N–S and $\pi/2$ is E–W.

Fig. 4 illustrate the dynamics of the flux during a diurnal cycle. Starting with little spatial variability during the night when little energy is available, the flux variance increases first in the East as the sun rises over the domain. Note the ridge at $\pi/2$ (90°) at 8 AM. By midday the fluxes show large, directionally dependent, spatial variations. As the sun sets the variance decreases across the Eastern portion of the domain first and then the Western portion.

At 1400 the directional semivariogram show maximum decorrelation at $\sim 2\pi/3$ and maximum correlation at $\sim \pi/4$. Note that several major homogeneous features are oriented at $\sim \pi/4$ across the calculation domain, i.e. the Atlantic coastline, the eastern mountain range, and the mid West agriculture regions. Thus the fluxes are relatively correlated (homogeneous) in this direction at all lag distances. In directions perpendicular to these features, $\sim 2\pi/3$, the variance increases rapidly at small lags and increases continually as the lag increases. Thus decorrelation occurs continuously with increased separation in directions that cross the major geographical features.

The semivariograms in Fig. 4 illustrate the lack of both spatial and temporal homogeneity in the surface fluxes of mercury across major portions of the US and Canada. This is the first time, to our knowledge, that the spatial variation in surface fluxes has been quantified. This emphasizes the value of HgSIM in capturing these

(a)

(b)

(c)

(d)
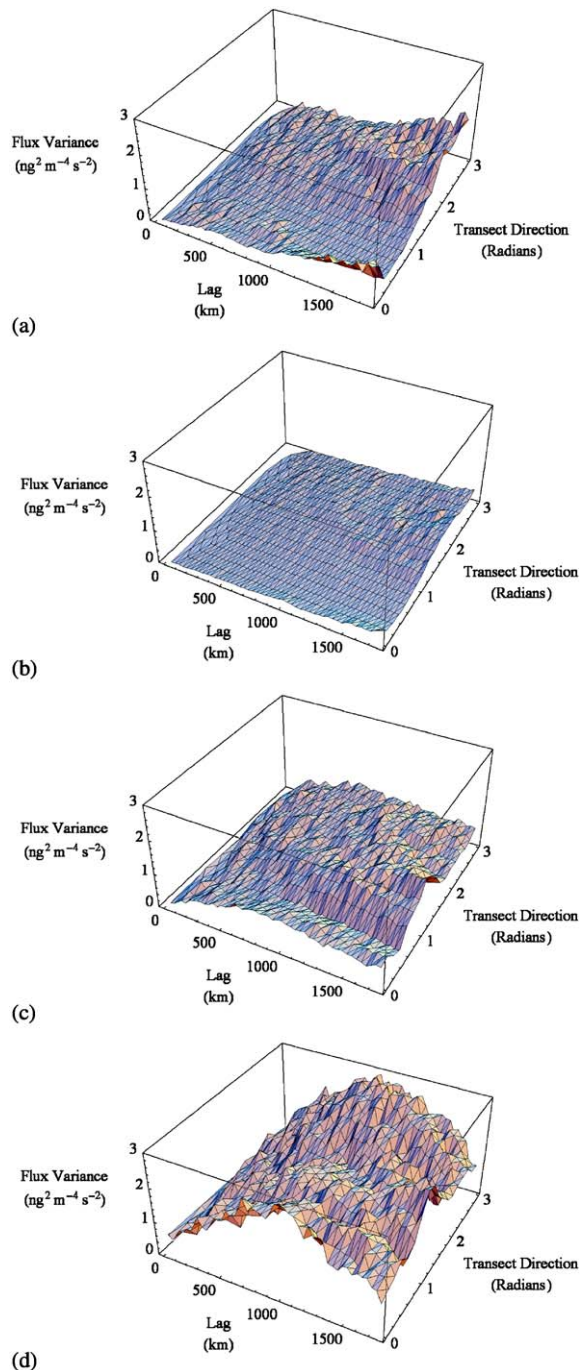
Fig. 4. (a–d) Directional semivariograms of mercury fluxes across the computational domain for the average July day for 0200, 0800, 1400, and 2000 EST.

variations and integrating them into the global scale processes. We plan to continue upgrading HgSIM as more measurements and knowledge of natural emissions

become available and using it to extrapolate new experimental findings.

5. Conclusions

HgSIM was used to estimate Hg^0 emissions from vegetation canopies, soil surfaces and water surfaces for a 2-week period in July 1997 for NE United States and SE Canada. The estimates from vegetation canopies, averaged over the 14 days, ranged from $0.0\,ng\,m^{-2}\,h^{-1}$ during the night time hours when transpiration ceased to $4.46\,ng\,m^{-2}\,h^{-1}$ during afternoon emissions in a mixed deciduous–coniferous forest. The range of the air–water flux was between 0.5 and $2.73\,ng\,m^{-2}\,h^{-1}$ over the model domain with the higher emissions rates corresponded to windier and warmer areas. The soil emissions ranged from near 0 to $2.3\,ng\,m^{-2}\,h^{-1}$ with the higher rates corresponding to warmer agricultural regions. Over the 2–week simulation the highest total natural emissions were $820\,ng\,m^{-2}$ from the Atlantic Ocean off the Southeast coastline and the lowest total biogenic emissions were $74\,ng\,m^{-2}$ in the urban areas with little vegetation cover around Washington DC. Recent published values from field measurements at uncontaminated sites were within the range of the estimated emissions from all three sources.

HgSIM modeled mercury fluxes are highly variable in both time and space. The spatial variations in the fluxes are due to the land use parameterization and the gradients in meteorological parameters over the large domain. Temporal variations occur with both diurnal cycles and larger synoptic cycles as weather systems pass over the modeled regions.

The average vegetation emissions rates for forested regions were roughly twice that of the soil or water emission rates during times of peak transpiration. However, the vegetation and soil emissions exhibit a strong diurnal pattern with lower emissions at night while the emissions from water do not. Therefore, the total emissions from the water over the 2-week period were roughly equal to that of vegetation emission from heavily forested areas. Emissions from soils below forest canopies contributed about 20–25% of the total forest emissions. In agricultural regions, direct emissions from soils were the largest source contributing up to 75% of the total terrestrial emissions in these locations.

This study showed that the spatial variability in mercury flux across the region was extreme and that spatially distributed models are the most feasible way to integrate and "scale-up" over large regions.

Finally, it should be noted that this model study does not include higher emissions from large areas around industrial centers which are likely to be more contaminated with Hg. If higher soil and water concentrations in these areas can be documented, their effect could be easily included in future HgSIM simulations.

References

Bash, J.O., 2003. A Model (HgSIM) for Biogenic Emissions of Mercury in the Northeast, United States. Thesis. Natural Resources Management and Engineering, University of Connecticut. 1376 Storrs Rd., Storrs, CT. O6269–4087 67p.

Bishop, K.H.L., Ying-Hua, Munthe, J., Dambrine, E., 1998. Xylem sap as a pathway for total mercury and methylmercury transport from soils to tree canopy in the boreal forest. Biogeochemistry 40, 101–113.

Campbell, G.S., Norman, J.M., 1998. An Introduction to Environmental Biophysics. Springer, New York 283pp.

Carpi, A., Lindberg, S.E., Hanson, P.J., Meyers, T.P., Kim, K.-H., 1998. Application of a teflon: tests and results over background soil. Atmospheric Environment 32 (5), 873–882.

Fitzgerald, W.F., 1995. Is mercury increasing in the atmosphere? The need for an Atmospheric Mercury Network (AMNET). In: Porcella, D.B., Huckabee, J.W., Wheatley, B. (Eds.), Mercry as a Global Pollutant. Kluwer Academic Publishing, Dordrucht, pp. 245–254 1312.

Gardfeldt, K., Feng, X., Sommar, J., Lindqvist, O., 2001. Total gaseous mercury exchange between air and water at river and sea surfaces in Swedish coastal regions. Atmospheric Environment 35 (17), 3027–3038.

Gillis, A.A., Miller, D.R., 2000. Some local environmental effects on mercury emission and absorption at a soil surface. The Science of The Total Environment 260 (1–3), 191–200.

Grell, G. A., Dudhia, J., Stauffer, D. R. 1994. Description of the Fifth Generation Penn State – NCAR Mesoscale Model (MM5). NCAR Technical Note: NCAR/TN-398 + STR. 138p.

Gustin, M.S., Lindberg, S.E., 2000. Assessing the contribution of natural sources to the global mercury cycle: The importance of intercomparing dynamic flux measurements. Fresenius Journal of Analytical Chemistry 366, 417–422.

Hanson, P.J., Lindberg, S.E., Tabberer, T.A., Owens, J.G., Kim, K.-H., 1995. Foliar exchange of mercury vapor: Evidence for a compensation point. Water, Air, and Soil Pollution 80 (1–4), 373–382.

Isaaks, E.H., Srivastava, R.M., 1989. An Introduction to Applied Geostatistics. Oxford University Press, New York 561pp.

Jarvis, P., 1976. The interpretation of the variations in leaf water potential and stomatal conductance found in canopies in the field. The Royal Society of London. Proceedings Series B(273), 593–610.

Lamborg, C.H., Fitzgerald, W.F., O'Donnell, J., Torgersen, T., 2002. A non-steady-state compartmental model of global-scale mercury biogeochemistry with interhemispheric atmospheric gradients. Geochimica et Cosmochimica Acta 66 (7), 1105–1118.

Lee, X., Benoit, G., Hu, X., 2000. Total gaseous mercury concentration and flux at a coastal salt marsh in Connecticut, USA. Atmospheric Environment 34, 4205–4213.

Lindberg, S.E., Hanson, P.J., Meyers, T.P., Kim, K.-H., 1998. Air/surface exchange of mercury vapor over forests-The need for a reassessment of continental biogenic emissions. Atmospheric Environment 32 (5), 895–908.

Lindberg, S.E., Dong, W., Meyers, T., 2002. Transpiration of gaseous elemental mercury through vegetation in a subtropical wetland in Florida. Atmospheric Environment 36 (33), 5207–5219.

Pirrone, N., Costa, P., Pacyna, J.M., Ferrara, R., 2001. Mercury emissions to the atmosphere from natural and anthropogenic sources in the Mediterranean region. Atmospheric Environment 35 (17), 2997–3006.

Poissant, L., Casimir, A., 1998. Water-air and soil-air exchange rate of total gaseous mercury measured at background sites. Atmospheric Environment 32 (5), 883–893.

Rolfhus, K.R., Fitzgerald, W.F., 2001. The evasion and spatial/temporal distribution of mercury species in Long Island Sound, CT-NY. Geochimica et Cosmochimica Acta 65 (3), 407–418.

Sanemasa, I., 1975. The Solubility of Elemental Mercury in Water. Bulletrin of the Japan Chemical Society 48, 1795–1798.

Stein, E.D., Cohen, Y., Winer, A.M., 1996. Environmental Distribution and Transformation of Mercury Compounds. Critical Reviews in Environmental Science and Technology 26 (1), 1–43.

Stewart, J.B., 1988. Modelling surface conductance of pine forest. Agriculture and Forest Meteorology 43, 19–35.

Stull, R.B., 1988. An Introduction to Boundary Layer Meteorology. Kluwer Academic Publishers, Boston MA 666p.

Thomann, R.V., Mueller, J.A., 1987. Principles of surface water quality modeling and control. Harber & Row, New York 644pp.

Wanninkhof, R., 1992. Relationship between wind speed and gas exchange over the ocean. Journal of Geophysical Research 97, 7373–7382.

Xu, X., Yang, X., R. Miller, D., Helble, J.J., Carley, R.J., 1999. Formulation of bi-directional atmosphere-surface exchanges of elemental mercury. Atmospheric Environment 33 (27), 4345–4355.

Zhang, H., Lindberg, S.E., Barnett, M.O., Vette, A.F., Gustin, M.S., 2002. Dynamic flux chamber measurement of gaseous mercury emission fluxes over soils. Part1: simulation of gaseous mercury emissions from soils using a two-resistance exchange interface model. Atmospheric Environment 36 (5), 835–846.

Zhang, H., Lindberg, S.E., Marsik, F.J., Keeler, G.J., 2001. Mercury air/surface exchange kinetics of background soils of the Tahquamenon River watershed in the Michigan Upper Peninsula. Water, Air, and Soil Pollution 126, 151–169.